Reprint

J.M. Costa, "Digital tomographic filters for radiographs", in *Multidimensional Systems: Techniques and Applications*, S.G. Tzafestas (Ed.). New York, N.Y.: Marcel Dekker, 1986, pp. 585-623.

13

Digital Tomographic Filters for Radiographs

JOSÉ M. COSTA Bell-Northern Research, Ltd., Ottawa, Ontario, Canada

1. INTRODUCTION

There are imaging technologies, such as those using x rays, in which the image consists of the superposition of many other images. This chapter considers the problem of conventional radiology, where a three-dimensional object is projected onto a two-dimensional film by means of x rays. If we think of the object as composed of a stack of layers, the images of these layers are all superimposed on the film. This is illustrated in Fig. 1, where the object has two layers. In conventional radiology, x rays are emitted from the focal spot of an x-ray tube in the form of a divergent beam (refer to Fig. 1), and traverse a three-dimensional body where they are attenuated in intensity due to the absorption in that body. Lack of imaging devices for x rays, such as lenses and mirrors, force the use of a shadow-casting geometry. A two-dimensional image, containing information from all depths in the object, is projected by these attenuated x rays. The x-ray image is converted into a light image by an intensifying screen in contact with the radiographic film (a screen-film combination), where the image is registered to form the radiograph. The relative position of the structures and objects that are in the body, whose images are all superimposed on the film, and the depth of those structures are not readily seen in the radiograph. Hence it would be very useful to have means of obtaining clear images of each layer in the body. This is important in diagnostic medicine for determining more precisely the nature and location of the lesions in the body.

The objective of this chapter is to provide a brief overview of some of the techniques that have been proposed to overcome this problem of three-dimensional imaging with x rays and to discuss in more detail how multidimensional digital filtering techniques could be used to improve the three-dimensional information in conventional radiographs. In particular, a new technique referred to as tomographic filtering is introduced and discussed.

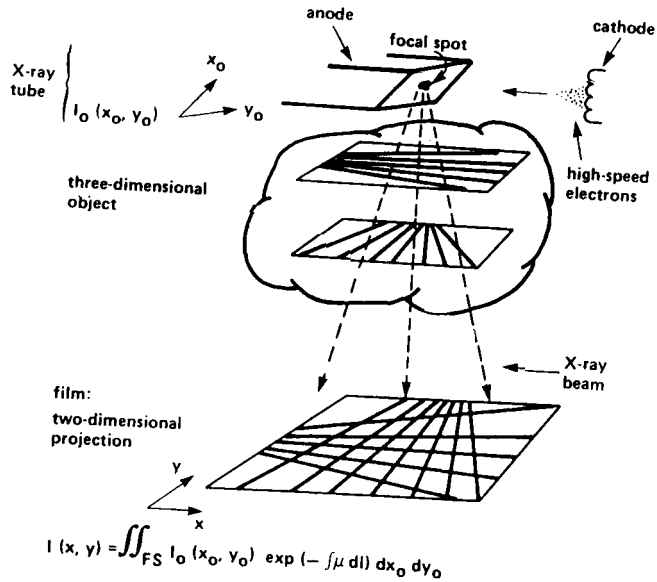

FIGURE 1 Conventional radiology.

The three-dimensional imaging techniques by means of x rays are summarized in Sec. 2 and the development of the tomographic filtering technique, including a review of conventional radiology, appears in Sec. 3. A comparative performance assessment of tomographic filtering with conventional radiology and standard tomography is also summarized in Sec. 3. In Sec. 4 the practical implementation of tomographic filters is discussed and examples of application to simulated radiographs are given. Finally, some conclusions and suggestions for further research are given in Sec. 5.

2. THREE-DIMENSIONAL IMAGING TECHNIQUES WITH X RAYS

Four techniques are briefly reviewed in this section: standard tomography (Sec. 2.1), computerized tomography (Sec. 2.2), coded x-ray sources (Sec. 2.3), and tomographic filtering (Sec. 2.4). Both standard tomography and computerized tomography are widely used in hospitals.

2.1. Standard Tomography

X rays were discovered in 1895 and as early as 1916 special radiographic techniques, based on moving x-ray tubes, were invented to obtain clear images of certain parts of a body by blurring redundant images of other

parts [1]. These techniques have been reinvented, modified, and improved over the years, and have received different names, such as laminagraphy, planigraphy, stratigraphy, body-section radiography, tomography, stereoradiography, classical motion tomography, and others [1-4]. Here they will be referred to as standard tomography.

Standard tomographic techniques produce a tomogram by moving a pointlike x-ray source and the recording film in a coupled manner, so that during the exposure the parts of the object lying in one specific plane parallel to the film plane are always projected on the same place on the film [1]. The x-ray shadows of the other parts of the object will move in relation to the film. Thus a layer of finite thickness at a predefined depth of the body is imaged sharply, whereas structures on both sides of this layer are blurred. The layer whose image is in focus is referred to as the plane of cut or tomographic layer.

A standard tomogram is actually the result of multiple radiographic exposures from different positions on a single film as the x-ray tube and film move. If multiple radiographic exposures (typically 8 to 20) were obtained on separate films, each at a different distance for a different tube position, films could be superimposed optically or electronically to bring into focus any plane [5,4, pp. 368-371]. This method has been referred to as tomosynthesis [6,7].

Standard tomograms suffer from the noise due to overlaying and underlaying layers, and attempts to eliminate it by removing defocus blur, using both optical and digital signal processing techniques, have been reported (e.g., [8-11]).

2.2. Computerized Tomography

Computerized tomography (CT) has been a major breakthrough in the development of x-ray imaging techniques in the 1970s [12]. CT is based on using multiple projections of a layer and a computer to reconstruct numerically the distribution of absorption coefficients in that layer. Since the x-ray beam is allowed to diverge in two dimensions only and solid-state detectors in the CT scanner have finite size, these two aspects together define the width of the layer. Additional collimation in front of the detectors reduces the signal from scattered x rays, which would produce noise from outside the plane. Thus the main advantages of CT over standard tomography are that only information for a given layer is obtained, without any significant noise from other layers, and that the information is obtained directly in digital form. Reviews of CT methods have been done by Mersereau [13,14], Robb [12], and others (e.g., [15,16]). Mersereau even proved that, in theory, bandlimited functions of finite order can be reconstructed exactly from a single projection. This is relevant because it would reduce the patient dose considerably; however, no practical system to reconstruct exactly three-dimensional information from a single projection is available yet.

Techniques are being investigated to enable computerized tomography to be carried out from a set of radiographs taken at different angles using conventional radiography units [17]. Since these units are available in many primary health care centers, they could be linked with a central medical computing facility to provide cost-effective access to processing and expert interpretation of the simulated CT images, for people in remote areas [17].

2.3. Coded X-Ray Sources

Another technique [18] uses a spatially modulated large-area x-ray source, which produces a shadow image of the object, but in a coded form. Since this type of source has an adequate high-frequency content, the coded image contains fine detail information which can be recovered by decoding it. Decoding is done using optical techniques and only a thin slice of the object is in focus at one time, but other slices may be brought into focus by changing lens positions in the reconstruction system. Alternatively, digital techniques can also be used in the reconstruction. One advantage of coded x-ray sources over standard tomography and CT is that no mechanical motion is required [4, p. 471]. However, a disadvantage is that the noise contributed by the out-of-focus planes during the reconstruction may be quite complex. Coded-source imaging is an outgrowth of the coded-aperture technique used in x-ray astronomy and nuclear imaging [19]. The spatially modulated x-ray source can be constructed using etching techniques. Although many shapes could be used, decoding is particularly simple if the pattern is a Fresnel zone plate [18].

2.4. Tomographic Filtering

One of the remaining challenges in radiology is to improve the diagnostic value of the billions of radiographs being produced in hospitals every year using conventional radiography equipment. Enhancement and restoration techniques have had limited practical application to the processing of radiographs in the past [20]. This has probably been due more to the inconvenience of their application (e.g., for digital processing the films must be digitized and for optical processing the optical system has to be set up) than to the limitations of the image processing techniques themselves. Ideally, to make use of the existing radiology equipment in conjunction with digital techniques, what would be needed is a new type of replacement cassette (the box that contains the screen-film combination), containing solid-state detectors which would produce a digital output directly. With the advent of digital radiography and image archival and communication systems (e.g., [21-24]), digital image processing techniques will be applied much more readily, because the images will already be digitized and the processing and display will be facilitated. However, little work has been published on the problem of recovering three-dimensional information from a single radiograph (see [13,14]). The tomographic filtering technique has recently been

proposed to simulate standard tomography using conventional radiology systems and digital signal processing techniques [25]. This approach to tomographic restoration of radiographs uses the depth-dependent focal-spot blur and it is described in detail in the rest of this chapter.

3. TOMOGRAPHIC FILTERS

Before any improvement of three-dimensional information in radiographs can be attempted, it is necessary to study the characteristics of the image formation process in radiology to find out what are the depth-dependent features. To date, almost all theory of conventional radiography has dealt with two-dimensional objects (see [4, p. 187]). The very nature of the radiologic process, however, forces one to consider three-dimensional objects in all imaging problems. The formation of the images of three-dimensional objects using conventional radiology is reviewed here (Sec. 3.1) and the concept of tomographic filtering is developed by establishing an analogy with standard tomography (Sec. 3.2). The transfer functions are examined (Sec. 3.3) and the performance of tomographic filtering is compared with conventional radiology and standard tomography (Sec. 3.4).

3.1. Review of Radiological Imaging

The radiological system may be modeled by a sequence of transformations intimately related in that the result of one forms the input to the next [26]. The degradations introduced at each stage of the radiological process have been studied in great detail from the point of view of image quality (e.g., [26-31]). Here the characteristics of the image formation process are briefly reviewed and modeled (a more in-depth review of the modeling of the radiological process may be found in [25,32]. Basically, there are six stages which may be modeled by transfer functions plus additive or multiplicative noise (see Fig. 1):

1. Electron gun: Electrons are generated by a heated filament (cathode) in the x-ray tube. They are focused and accelerated at high speed toward the target (anode) [33]. The angle formed by the target surface and the direction of the center x ray is referred to as the target angle.

2. Focal spot: The region in the target where the x rays and the heat are produced is called the focal spot. Many studies have been published about the characteristics of focal spots in x-ray tubes (e.g., [34-39]. The shape and size of focal spots have been determined as well as their modulation transfer functions (MTFs) and impulse responses or point-spread functions (PSFs), both theoretically and experimentally. The MTF of a focal spot resembles a gaussian function [35,37,40]. It is usually double-peaked and this introduces phase shifts in the image [41]. The randomness in the generation of x rays (photons) has been referred to as quantum mottle (see [31]).

3. X-ray image formation: The interaction of x rays with matter may be modeled by

$$I(z) = I(0) \exp\left[\int_0^z -\mu(\ell)\, d\ell\right] \quad (1)$$

where I(z) is the intensity of a narrow x-ray beam from a point source as a function of the distance z in the direction of propagation, and $\mu(\ell)$ is a total attenuation coefficient in that direction. Since this interaction is the key to the whole process of three-dimensional restoration, it is analyzed in more detail below. Scattered radiation (see [42]) is considered as noise and it is not too relevant here, because it does not contribute to differentiate among layers.

4. Imaging system: The imaging system records the x-ray image on the radiological film, by means of an intensifying screen which converts the x-ray image into a light image (alternatively, electronic image intensifiers can be used [43]). In addition to the low-pass characteristics of the frequency response of the imaging device, the main distortions in the recording and display of images are due to random noise and nonlinearities [44-48].

5. Restoration and enhancement: Although image processing operations do not yet exist in most systems of conventional radiology, as discussed previously, they will become increasingly important as electronic acquisition and digital image archiving and retrieval are applied to medicine (see [22-24,43]). In laboratory experiments, both restoration [49] and enhancement [50] techniques have been applied to radiographs (e.g., [20,44,51-54]). Several researchers have investigated the removal of penumbras in radiographs using optical signal processing techniques [55-57].

6. Pattern recognition process: The recognition of patterns by a radiologist results in a diagnosis. In certain cases the pattern recognition may be done with the aid of a computer (e.g., [58,59]).

An analysis of all these transformations has shown that the only effects that could be useful for obtaining three-dimensional information are due to the finite size of the focal spot and the diverging nature of the x-ray beam [25]. Thus it is important to examine this more closely:

Interaction of X Rays with Matter

X rays propagate in straight lines. This fact controls the size, shape, and position on the radiographic film of the shadow or image of the various structures of the object being exposed. Due to the diverging nature of the x rays emitted by the focal spot, the image of the object is magnified. With reference to Fig. 2, the magnification for the layer at depth z_i is

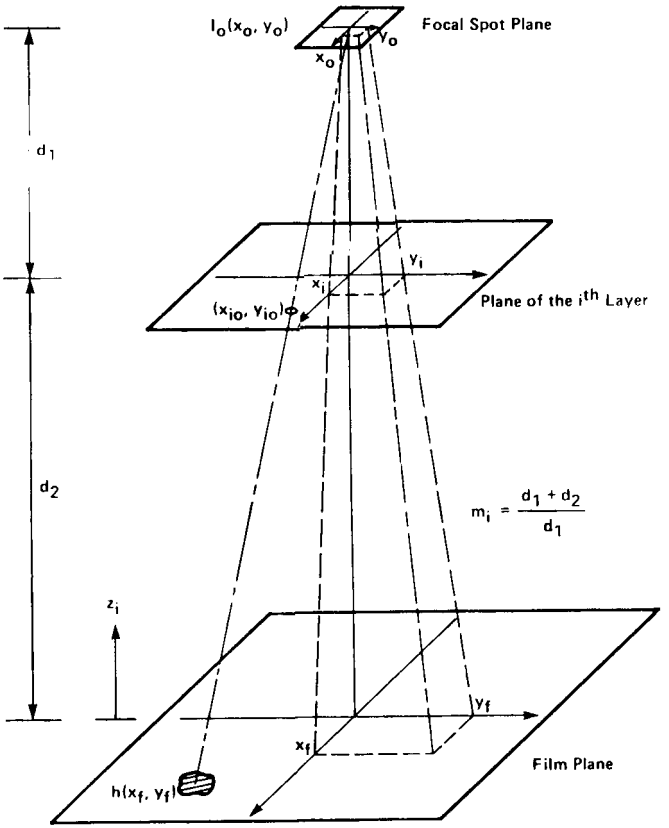

FIGURE 2 Impulse response formation.

$$m_i = \frac{d_1 + d_2}{d_1} \tag{2}$$

which is a constant for each layer parallel to the film plane.

The x-ray image intensity distribution that reaches the imaging system is a function of both the distribution of absorption coefficients in the object and the x-ray intensity distribution in the focal spot. Let $I_0(x_0,y_0; x_f,y_f)$ by the x-ray intensity emitted from the point (x_0,y_0) in the focal spot toward the point (x_f,y_f) in the film. The spatial distribution of absorption coefficients in the object is denoted by $\mu_L(\ell)$, which is defined along a line L from (x_0,y_0) to (x_f,y_f), for all possible L. The interaction between these two functions or inputs to the system can then be modeled by the following integral equation:

$$I(x_f,y_f) = \int\int_{F.S.} I_0(x_0,y_0;x_f,y_f) \exp\left[-\int_L \mu_L(\ell)\, d\ell\right] dx_0\, dy_0 \quad (3)$$

which is a generalization of (1) and is obtained by integrating over the region of the focal spot (denoted here by F.S.). This equation is valid with any function I_0 and any three-dimensional object, in general.

From (3) it is clear that the radiologic process is linear with respect to I_0 and nonlinear with respect to the attenuation coefficients μ. Nevertheless, an approximation can be made because the values of the linear attenuation coefficients, or at least their variations from point to point, are small and the exponential in (3) can be approximated by the linear terms of its Taylor series expansion [60,61]. Once the system is linearized it can be described by convolution integrals if the system is also space invariant. However, the radiologic system is space variant for several reasons, such as the divergent nature of the x-ray beam, the superposition of images of the layers in the object, the lack of parallelism of the focal spot and film planes, and the change of the x-ray intensity emitted from the focal spot with direction.

Some solutions can be devised to make the space-variant problem tractable [25,62]. The effect of the divergent nature of the x-ray beam when it reaches the film is that the intensity has been distorted according to the inverse square law. Since the consequences of this effect are deterministic, the intensity in the image can be corrected with image processing algorithms. Nevertheless, if the distances to be considered on the film plane are small, this effect can be neglected, because in radiology the focal spot to film distance is much greater than the focal spot size, say 1000:1. To deal with the problem of the varying intensity $I_0(x_0,y_0;x_f,y_f)$ of the x rays emitted from the focal spot if they are different in each direction, the image could be divided into small sections within which the impulse response could be assumed to be constant [63]. If a mathematical relationship between intensity and direction did exist, it would then be possible to correct the image intensity automatically, as in the case of the inverse-square-law correction. However, in practical applications the intensity is normally the same in all directions, so that this correction is not necessary and the intensity becomes $I_0(x_0,y_0)$, a function of (x_0,y_0) only. $I_0(x_0,y_0)$ is referred here to as the exposure function. The lack of parallelism of the focal spot and the film also makes the system space variant. The PSF has different size and shape everywhere in the space, even within the same layer. A solution has been proposed to correct for this problem [25], where a new image is calculated by interpolation in a plane parallel to the focal spot, and thus it has space-invariant properties. The equations of this transformation and the conditions under which it should be applied are given in [25,32].

$I_0(x_0,y_0)$ can be determined by exposing an object with a known distribution of absorption coefficients [64]. If the object is a pinhole, the system impulse response $h(x_f,y_f)$ is obtained. The size of the pinhole should be of

no more than a few micrometers in diameter [65]. It can be shown [25] that the exposure function $I_0(x_0,y_0)$ is then given by

$$I_0(x_0,y_0) = h\left(\frac{d}{d_1} x_{i0} - \frac{d_2}{d_1} x_0, \frac{d}{d_1} y_{i0} - \frac{d_2}{d_1} y_0\right) \tag{4}$$

where (x_{i0},y_{i0}), d_1, and d_2 determine the position of the pinhole, and $d = d_1 + d_2$ (see Fig. 2). Once the exposure function is known, the problem consists of recovering the spatial distribution of absorption coefficients based on (3) and given a two-dimensional projection, the image $I(x_f,y_f)$. This is not an easy task, as discussed previously. Conventional radiography masks the depth information by giving a shadow-cast image of the body, which contains hidden parts, blur due to the convolution with I_0, and noise. The purpose of tomographic filtering is to improve the image of one layer with respect to the others.

3.2. Tomographic Filtration Process

A tomographic filtration process (TFP) must produce a focusing effect similar to that of standard tomography, but using conventional radiology equipment and with no moving parts. In a TFP, instead of moving the x-ray tube, the finite size of the focal spot is used to advantage, and instead of moving the film, a filter is used to process a conventional radiograph. To see that a TFP is indeed analogous to a standard tomographic system in miniature, as far as the tomographic layer is concerned, consider the following model.

A focal spot is composed of a finite ordering of point sources. Each emitting source produces its own image at a slightly different point in the image plane [66]. The shadows from all these point sources add up to form the observed image; overlapping occurs throughout the entire image but will be discernible only at the edges, where an intensity gradient is formed. Since this system is linear we can apply superposition and make an equivalent focal spot by moving a true point source of x rays over a region that includes the real focal spot. With this model (3) is still valid, but F.S. would now denote the movement of a point source. The movement of this point source is analogous to the movement of an x-ray tube in standard tomography. Since in conventional radiology the film does not move, the images of all the layers are blurred. Therefore, in order to convert a radiograph into a tomogram we will pass the radiographic image through a filter. Filters that produce a selective deblurring on a conventional radiograph will be referred to as tomographic filters. While tomographic filtering usually refers to the filter or process that produces tomographic restoration, the term TFP refers to the complete system, including the conventional radiology equipment (see Fig. 3).

Since a typical size for the focal spot is of the order of 2 mm, while the movement of an x-ray source in standard tomography is of the order of

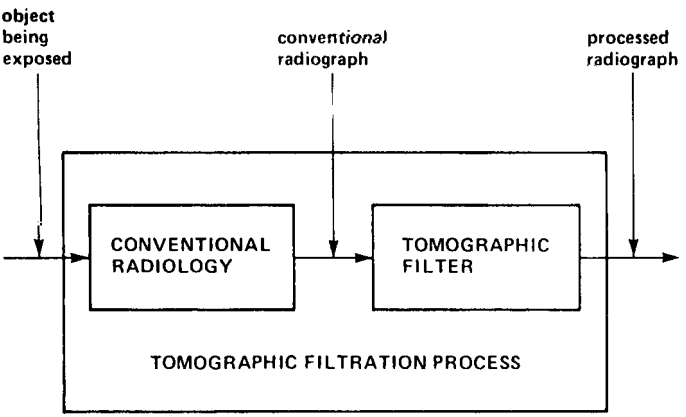

FIGURE 3 Concept of tomographic filtering.

500 mm, we infer that a TFP would be more comparable to zonography. Zonography is essentially standard tomography using small displacements of the x-ray source, of the order of a few millimeters [3, Chap. 14], [67, 68]. Other comparable narrow-angle tomographic techniques are stereozongraphy, narrow-angle stratigraphy, and orthotomography [3, pp. 7-8, 300-311].

To derive the transfer function of a tomographic filter, the frequency-domain equations of image formation in radiography had to be derived for three-dimensional objects. To make the results more general and allow comparisons between systems, the model of conventional radiology was derived as a special case of standard tomography. This derivation was motivated by that in [60]. Some of the constraints in [60] were removed, namely, the linear movement of a constant-intensity x-ray source, while others relevant to this application were added, namely, small displacements of the x-ray source. Nevertheless, none of these constraints imply a lack of generality in the derivation.

Consider the diagram of standard tomography shown in Fig. 4. The reference coordinate systems whown in Fig. 4 are self-explanatory: x_0,y_0 is the x-ray source plane, x_t,y_t is the plane of cut, x_i,y_i is any layer in the object at depth z_i (z_i is its distance to the film plane), x_f,y_f is the (moving) film, and x,y is the (fixed) plane containing the film. In this model, the x-ray point source (X) can move anywhere in the plane x_0,y_0 parallel to the film plane, and the intensity during this trajectory is given by the exposure function $I_0(x_0,y_0)$. In standard tomography the film also moves in synchronism with the x-ray source to keep the desired plane of cut x_t,y_t in focus, according to the following relationship:

$$x = x_c + x_f = -\left(\frac{D_2}{D_1}\right)x_0 + x_f$$

$$y = y_c + y_f = -\left(\frac{D_2}{D_1}\right)y_0 + y_f$$

It is not possible to reproduce here all the details of the derivation, which can be found in [25,32]. However, it is important to recap the approximations made:

1. The x-ray intensity from (x_0,y_0) to (x_f,y_f) is independent of (x_f,y_f) and the position of the film.
2. If the displacements of the x-ray source are small compared to the distance from the source to the plane of cut, a differential length along

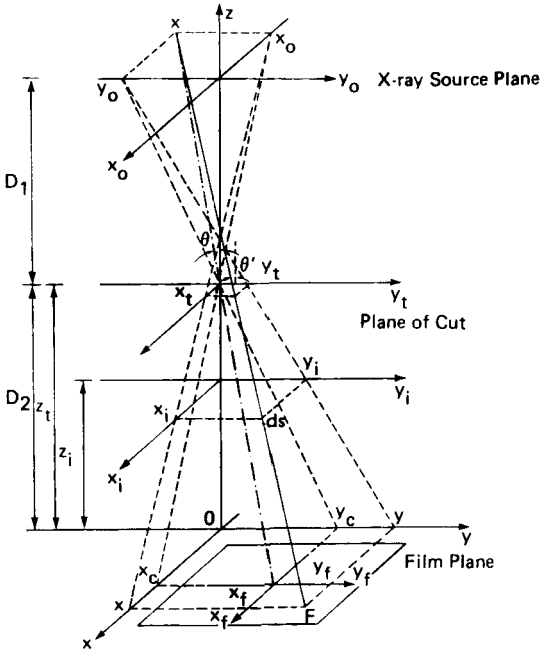

FIGURE 4 Coordinates in standard tomography.

the x-ray path ($d\ell$) can be replaced by the corresponding vertical differential length (dz_i).

3. Since the values of the linear attenuation coefficients, or at least their variations from point to point, are small, the exponential representing the attenuation of x rays through matter [recall (1) and (3)] can be approximated by the linear terms of its Taylor series expansion [60,61].

Considering these approximations and applying the Fourier transform to (3), the final result is

$$G(f_x,f_y) = I_B\delta(f_x,f_y) - \int_0^d H_i(f_x,f_y,z_i)F_\mu(f_x,f_y,z_i)\,dz_i \tag{5}$$

where $G(f_x,f_y)$ is the Fourier transform of the resulting image on the film $I(x_f,y_f)$; I_B is a constant; $\delta(f_x,f_y)$ is the Dirac delta function; $H_i(f_x,f_y,z_i)$ is the transfer function of the ith layer, at a distance z_i from the film, as given in (6) for standard tomography; and $F_\mu(f_x,f_y,z_i)$ is the two-dimensional Fourier transform of the attenuation coefficients $\mu(x_i,y_i,z_i)$ at depth z_i, as given in (7):

$$H_i^{ST}(f_x,f_y,z_i) = \left[\frac{z_i - d}{z_i - D_2}\,\frac{D_1}{d}\right]^2 \int\int I_0\left(\frac{z_i - d}{z_i - D_2}\,\frac{D_1}{d}x,\ \frac{z_i - d}{z_i - D_2}\,\frac{D_1}{d}y\right) \times e^{-j2\pi(f_x x+f_y y)}\,dx\,dy \tag{6}$$

$$F_\mu(f_x,f_y,z_i) = \int\int \mu\left(\frac{d - z_i}{d}x,\ \frac{d - z_i}{d}y, z_i\right)e^{-j2\pi(f_x x+f_y y)}\,dx\,dy \tag{7}$$

where D_1 and D_2 determine the position of the plane of cut. The transfer function of the plane of cut [i.e., when $z_i = D_2$ in (6)] is a constant and its impulse response is an impulse, as expected by intuition (see Fig. 4). This results in a sharp image of the tomographic layer.

Equation (5) already suggests that the plane of cut can be changed by filtering the image. Indeed, suppose that there is interest in the plane at a depth $z_i = z_t$. Dividing both sides of (5) by $H_i^{ST}(f_x,f_y,z_t)$, the new overall transfer function for the layer at depth z_t is a constant; thus this layer has become the new plane of cut. The overall transfer function of the plane previously in focus ($z_i = D_2$) is now $\{H_i^{ST}(f_x,f_y,z_t)\}^{-1}$. The overall transfer for any other layer (i.e., at depth z_i) is now

$$\frac{H_i^{ST}(f_x,f_y,z_i)}{H_i^{ST}(f_x,f_y,z_t)}$$

Conventional radiology may now be considered as a special case of standard tomography. To derive the equation of conventional radiology, consider a radiologic system with focal spot intensity distribution $I_0(x_0,y_0)$ and focal spot to film distance $d = D_1 + D_2$. The diagram in Fig. 4 still applies by letting $D_2 = 0$ (i.e., the film does not move: $x = x_f$ and $y = y_f$) and substituting the movement of the point source of x rays in standard tomography for the intensity distribution of the finite-size focal spot. Under these conditions all the derivations leading to (5) and (6) are still valid, but with $D_2 = 0$. It should be noted, however, that the exposure function $I_0(x_0,y_0)$ is substantially different, although mathematically it makes no difference. Thus in conventional radiology the transfer function to be used in (5) is given by

$$H_i^{CR}(f_x,f_y,z_i) = H_i^{ST}(f_x,f_y,z_i)\Big|_{D_2=0} \tag{8}$$

Therefore, the mathematical models of standard tomography and conventional radiology are similar, but with different transfer functions. In conventional radiology none of the transfer functions for any layer is identically equal to a constant, except in the limiting case that $z_i = 0$ (film plane).

As before, the radiograph can be filtered so that the overall transfer function of one of the layers is equal to a constant, thus converting a radiograph into a tomogram. Hence the equation of a tomographic filtration process is the same as (5), but with the transfer function H_i given by (9):

$$H_i^{TF}(f_x,f_y,z_i) = H_t(f_x,f_y)H_i^{CR}(f_x,f_y,z_i) = \frac{H_i^{CR}(f_x,f_y,z_i)}{H(f_x,f_y)} \tag{9}$$

where

$$H_t(f_x,f_y) \triangleq \frac{1}{H(f_x,f_y)} \triangleq \frac{1}{H_i^{CR}(f_x,f_y,z_i)}\Bigg|_{z_i=z_t} \tag{10}$$

and where z_t is the depth of the layer to be deblurred by the tomographic filter [25]. Equation (10) shows that the transfer function of the tomographic filter $H_t(f_x,f_y)$ is *the inverse* of the transfer function for conventional radiology given in (8) and with $z_i = z_t$, the depth of the desired plane of cut.

Consequently, it has been shown that by comparing the movement of a point x-ray source with a finite-size focal spot and replacing the movement of the film in standard tomography by filtering a conventional radiograph, an analogy between standard tomography and tomographic filtering can be established.

It is interesting to note that the mathematical equations of conventional radiology, standard tomography, and tomographic filtering are similar. Nevertheless, there are fundamental physical differences among these methods [25,32]. The exposure function $I_0(.,.)$ in conventional radiology and tomographic filtering is defined over the area of the focal spot and the edges of this intensity distribution are not sharp, as discussed previously. On the other hand, in tomography, $I_0(.,.)$ defines the movement of a point-like x-ray source which is turned on and off over a line which can be straight, circular, elliptical, spiral, hypocycloidal, and so on. This means that the blur in conventional radiology is more uniform in all directions than in standard tomography. The uniformity of the blur is the reason why the more complicated x-ray source movements are preferred in tomography; the scanning of an area by an x-ray source has also been considered in tomography and it has been referred to as areal tomography [69, p. 63]. Of course, the source of x rays in tomography is also of finite size, but the blur that this produces is generally negligible compared to the blur due to its movement.

The nature of the processes themselves are also different. Indeed, the transfer functions of conventional radiology and standard tomography correspond to truly radiologic procedures, while the transfer function of a tomographic filtration process has a component (the denominator) which corresponds to an image processing operation (inverse filtering). This means that the errors and noise are of different nature in each case. In standard tomography additional blur or errors occur if the patient moves during the exposure or there are mechanical misadjustments. On the other hand, in a tomographic filtration process the effect of a patient moving is not so critical because the exposure time is much shorter, but the filtering process is not ideal in practice and noise may be amplified by the inverse filter, especially at high frequencies, where the gain is greater.

Tomographic filters will require new ways of examining images interactively with an image processor. In addition to the normal human factors, an important consideration in image processing when images are to be judged by the human eye is the psychophysics of vision [70,71]. For example, the mean-squared-error criterion is in very poor accord with subjective evaluation [47], and phase accuracy is extremely important in image processing filters [72].

Tomographic filters could be readily applied when on-line medical image communication systems [73] are available in hospitals, which will facilitate the storage, retrieval, processing, and display of images.

3.3. Variation of the Transfer Function with Depth

Ideally, a tomographic filter should have a frequency response such that in combination with the transfer function of the radiologic system, the resulting overall transfer function would be equal to a constant for the tomographic layer and equal to zero everywhere else. In practice, the second condition cannot be met, not even closely. It is the purpose of this analysis to investigate the overall frequency response at different depths.

The overall transfer function for a particular layer is equal to the quotient of the transfer function for that layer without the tomographic filter and the transfer function of the tomographic layer [see (9) and (10)]. Evidently, for the tomographic layer the overall transfer function is identically equal to a constant. The overall transfer function for other layers was analyzed and it is shown in Fig. 5. For simplicity and without loss of generality, one-dimensional functions are considered in Fig. 5. Since the shape of the transfer function is low-pass and its bandwidth increases with depth, it is clear that the tomographic filter acts as a low-pass filter for layers between the plane of cut and the focal spot, and as a high-pass filter for layers between the plane of cut and the film. This analysis can also be applied to any inverse filtering problem in which the inverse filter has a scaling error.

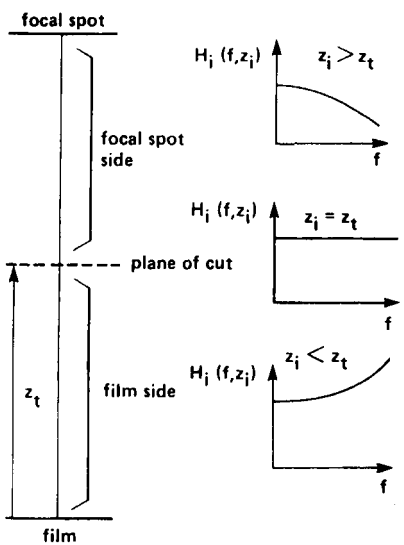

FIGURE 5 Variation with depth of the overall magnitude response in a TFP. (From Ref. 25.)

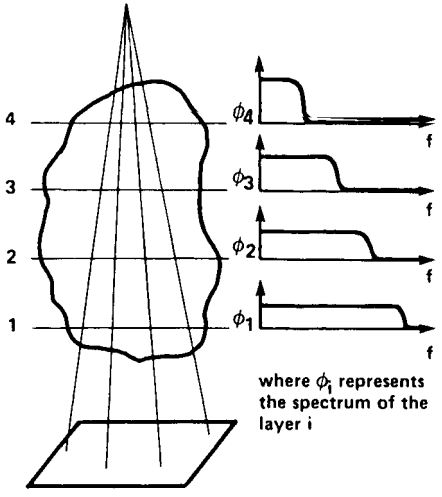

FIGURE 6 Scaling of the spectra of the images of layers at various depths.

Since radiographs consist of the superposition of the images of many layers, to understand the effects of radiograph processing fully we must also consider the composition of the spectrum of the projected object. Since different layers suffer different magnifications during exposure, the corresponding two-dimensional Fourier transforms of their shadow images are scaled accordingly. Assuming that each layer has the same spectrum, the relative scalings during magnification are shown in Fig. 6 (for simplicity they are shown in one dimension only). These different scalings of the shadow images of the layers in the object make the processing of radiographs more interesting. For example, a low-pass filter would enhance the images of the layers closer to the focal spot, while a high-pass filter would enhance the images of layers closer to the film. With band-pass or spectral-shaping filters in general, selective enhancement of certain layers could be realized. This is referred to as tomographic enhancement (as opposed to tomographic restoration, which has been described in this chapter).

3.4. Performance Comparison

The transfer functions contain all the information necessary to compare the various systems. However, they are inconvenient to calculate and compare. The first simplification is to ignore the phase transfer function and consider only the magnitude transfer function, usually referred to as the modulation transfer function (MTF). Nevertheless, for ease of comparison single-number parameters are commonly used in radiology. Tomographic filtering

has been compared with standard tomography/zonography and conventional radiology on the basis of the following parameters: the exposure angle, the thickness of the tomographic layer, the rate of change of the modulation transfer function, the signal-to-noise ratio, and the patient dose [25,74,75]. The conclusion of that comparative assessment is that tomographic filtering can be an improvement over conventional radiology, but cannot achieve the results of standard tomography. The main advantage of tomographic filtering is in reducing the radiation dose to the patient. These analytical results have been corroborated practically by processing both simulated radiographs and actual radiographs [25,76]. A brief summary of the comparative assessment of tomographic filtering follows, and pictorial examples are given below (Sec. 4).

Thickness of the Tomographic Layer

In standard tomography the thickness of the cut is normally defined as the distance between two levels which have a tomographic blurring that is insufficiently large to be noticeable in the presence of the usual radiographic blurrings. This is a subjective definition and depends on the relative amount of other blurrings, such as those due to the focal-spot intensity distribution and patient movement. On the other hand, in a tomographic filtration process (TFP) the tomographic blur is based on the focal spot intensity distribution, and the blur due to patient movement is negligible because the exposure time is very short.

Hence the thickness of the cut depends on the extent of the movement of the x-ray source in tomography or the size of the focal spot in a TFP. It is more usual to give the exposure angle rather than the extension of the movement of the x-ray source (or size). The exposure angle is defined as the angle through which the projecting ray of a central point of the plane of cut "moves" during the exposure. In tomography the exposure angle normally ranges from 1 to 5° (in zonography) to 120 to 170° (in transversal tomography) [3]. In conventional radiography, and therefore in a TFP, the exposure angle is determined by the size of the focal spot. With a typical focal spot size of 2 mm and focal spot to plane distance of 1000 mm, the exposure angle is about 0.1°. Thus, in terms of the exposure angle, a TFP would be closer to zonography than to any other tomographic technique.

When exposure angle is translated to thickness of cut, in standard tomography it is of the order of a few millimeters, in zonography it is of the order of a few centimeters, and in a tomographic filtration process even larger. Due to the lack of experimental data, conclusive results cannot be given for a TFP [25]. However, it is expected that by using visual workstations for interactive viewing (e.g., with zooming and magnification) the apparent thickness of cut in a TFP could become close to that of zonography. A TFP is an improvement over conventional radiography, but it cannot achieve the thin cuts of standard tomography.

The Rate of Change of the Modulation Transfer Function

A measure has been proposed to quantify the contrast between layers after they have been imaged on the film [25]. This is based on the rate of change of the transfer functions in (6), (8), and (9) from layer to layer for a specific type of exposure function $I_0(x_0,y_0)$. Quantitative results were obtained by assuming a single-peaked gaussian function in all three cases. This may not be realistic, but it provides a good basis to compare the performance of the tomographic filtration process with that of standard tomography. When identical exposure functions are considered, the results showed that for layers between the focal spot and the plane at a distance $(dz_t)/(2d - z_t)$ from the film, the transfer function in a TFP varies faster from layer to layer than in the equivalent system using standard tomography. It can be shown that this interval always contains the plane of cut $z_i = z_t$, hence in a region around the tomographic layer a TFP gives better contrast between layers than standard tomography. However, if the normal sizes of the exposure function are taken into consideration (i.e., about 500 mm in standard tomography and about 2 mm in TFP), the performance of standard tomography is by far better because the interval around the plane of cut is negligible.

The Signal-to-Noise Ratios

The signal-to-noise ratio (SNR) is defined here as the ratio of the power of the signal from the tomographic layer if it was the only one present in the object and the power of the noise contributed by all other layers. The signal-to-noise ratio provides another measure of the contrast of the image of the plane of cut with respect to the others.

The object being x-rayed, represented by the distribution of linear attenuation coefficients, is considered to be a random process. The power is given by the integral of its power spectral density function. To determine the signal-to-noise ratio the power component due to the image of the tomographic layer (P_t) and the noise power due to the other layers (P_n) are separated. It is also useful to separate the noise power due to layers between the anode and the tomographic layer (P_a) and the noise power due to layers between the tomographic layer and the film (P_f). Equation (11) shows how they are related:

$$P = P_t + P_n = P_t + P_a + P_f \tag{11}$$

Formulas to calculate these powers can be found in [25,75]. The various signal-to-noise ratios can then be calculated as follows:

$$SNR = \frac{P_t}{P_n} \tag{12}$$

$$SNR_a = \frac{P_t}{P_a} \tag{13}$$

$$SNR_f = \frac{P_t}{P_f} \tag{14}$$

$$SNR = \frac{SNR_a \times SNR_f}{SNR_a + SNR_f} \tag{15}$$

Equations (11) to (15) were calculated in about 4000 cases. Table 1 shows a representative sample of the results: the variation of the signal-to-noise ratio with respect to the nominal thickness of the tomographic layer. To calculate Table 1 the following parameters were assumed: d = 1000 mm, z_t = 500 mm, object of thickness 264 mm and positioned at equal distances

TABLE 1 Signal-to-Noise Ratios Versus the Thickness of the Cut

	Thickness of the cut (mm)					
	4	20	40	100	200	240
Standard tomography						
SNR	0.017	0.089	0.19	0.67	3.6	11.
SNR_a	0.033	0.18	0.39	1.3	7.1	23.
SNR_f	0.033	0.18	0.39	1.3	7.1	23.
Conventional radiography						
SNR	0.015	0.081	0.18	0.60	3.1	9.8
SNR_a	0.036	0.19	0.43	1.5	8.3	27.
SNR_f	0.026	0.14	0.3	0.99	4.9	15.
Tomographic filtering						
SNR	0.013	0.068	0.15	0.48	2.3	7.4
SNR_a	0.045	0.24	0.55	2.1	13.	47.
SNR_f	0.018	0.093	0.2	0.62	2.8	8.7

from film and focal spot, object made of white noise bandlimited at 5 cycles/mm, and $I_0(x_0,y_0) = \exp(-100x^2 - 100y^2)$.

The SNR (also SNR_a and SNR_f) increases with the thickness of the tomographic layer, as expected, because of its definition. Other results have shown that when the object is moved closer to the focal spot or the size of the exposure function increases, the SNR increases in standard tomography, but in conventional radiography and tomographic filtering it decreases [25]. When the system parameters are the same (i.e., any colmun in Table 1) SNR_a is maximum for tomographic filtering and minimum for standard tomography. On the other hand, SNR_f and SNR are maximum for standard tomography and minimum for tomographic filtering. This shows that tomographic filters perform better for layers in the object closer to the film. When the tomographic layer is closer to the focal spot, the high-pass effect on the layers on the side of the film produces the decrease in SNR through an increase in the noise power.

These measures give only an indication of the performance from a theoretical point of view. In practice, the object is very structured and the effects of noise due to other layers cannot be calculated statistically.

The Radiation Dose

The goal in radiagnostic radiology is to obtain as much relevant information as possible from inside a patient's body, while keeping the total radiation dose to a minimum to reduce any possible danger to the patient. Each radiologic procedure represents a compromise between dose and image and diagnostic qualities [77]. Standard tomography must be regarded as a relatively high-dose procedure and it is used only when there are specific indications which outweigh the risks [3, p. 314]. The radiation dose per exposure, typically 1 to 2 rad, is comparable to conventional radiology, but the total dose is usually greater since multiple exposures are the rule because the position of the relevant structures is not usually known.

Here the advantage of tomographic filtering is clear. With a single radiograph and tomographic filtering operations of different parameters, various images can be produced from which indications of the positions of the structures can be obtained. Once they are known, a subsequent thin-section tomogram at the proper depth using standard techniques may give a more accurate representation.

4. DESIGN AND REALIZATION OF TOMOGRAPHIC FILTERS

In order to implement tomographic filters, the transfer function in (10) is to be applied to the radiological image represented by $G(f_x,f_y)$ in (5) (see [25,32]).

$$F(f_x,f_y) \triangleq \frac{G(f_x,f_y)}{H(f_x,f_y)} = I_B \frac{\delta(f_x,f_y)}{H(f_x,f_y)} - \int_0^d \frac{H_i(f_x,f_y,z_i)}{H(f_x,f_y)} F_\mu(f_x,f_y,z_i)\, dz_i \quad (16)$$

where $F(f_x,f_y)$ is the Fourier transform of the radiographic image after it has been processed with a tomographic filter.

In this section we examine the process of designing a digital filter with transfer function $H_t(f_x,f_y)$ as given by (10). The approach used is inverse filtering, which is not the best but the simplest. Four steps are considered: determination of the function I_0 and the system impulse response (Sec. 4.1), noise handling techniques (Sec. 4.2), determination of the coefficients of the digital filter (Sec. 4.3), and implementation considerations, including examples (Sec. 4.4).

4.1. System Impulse Response

To determine $H_t(f_x,f_y)$ as given by (10), the following information is needed:

1. The distance d between the focal spot and the film when the object is imaged
2. The depth z_i of the layer of interest in the object that has to be deblurred
3. The exposure function $I_0(x_0,y_0)$

As discussed previously [see (4)], the exposure function $I_0(x_0,y_0)$ can be obtained by imaging an object with a known distribution of absorption coefficients, such as a pinhole. The pinhole approximates a delta function and thus the system impulse response or point-spread function (PSF), $h(x_f,y_f)$, is obtained.

Actual PSFs were obtained using the pinhole method and the x-ray equipment of the Radiological Research Laboratories, University of Toronto. Contour and perspective plots of a typical PSF and its squared modulation transfer function (MTF) are shown in Fig. 7. The nominal size of this focal spot was 1 mm. The x-ray film was digitized and the squared MTF was calculated using a two-dimensional FFT [25].

As will be discussed later, it is convenient to approximate the PSF by a separable function to save computer memory in the design of a tomographic filter. We have chosen a separable approximation in the frequency domain. Denote the PSF by $h(x_f,y_f)$ and its two-dimensional Fourier transform by $H(f_x,f_y)$. Then define a separable PSF $h_s(x_f,y_f)$ as

$$h_s(x_f,y_f) = h_x(x_f)h_y(y_f) \quad (17)$$

where

$$h_x(x_f) = \mathcal{F}^{-1}\{H_x(f_x)\} \triangleq \mathcal{F}^{-1}\{H(f_x,0)\}$$

$$h_y(y_f) = \mathcal{F}^{-1}\{H_y(f_y)\} \triangleq \mathcal{F}^{-1}\{H(0,f_y)\}$$

The separable two-dimensional Fourier transform of $h_s(x_f,y_f)$ is then

$$H_s(f_x,f_y) = H_x(f_x)H_y(f_y) = H(f_x,0)H(0,f_y) \tag{18}$$

According to the projection-slice theorem [14], this approximation keeps invariant the projections of the PSF along the x axis and y axis. This results also in further advantages, such as a smoothing of the PSF and reduced computer time. The result of this approximation on the PSFs of Fig. 7 is shown in Fig. 8.

The transfer function $H_t(f_x,f_y)$ is then calculated according to (10) and can be implemented using digital (see [25]) or optical (see [55,

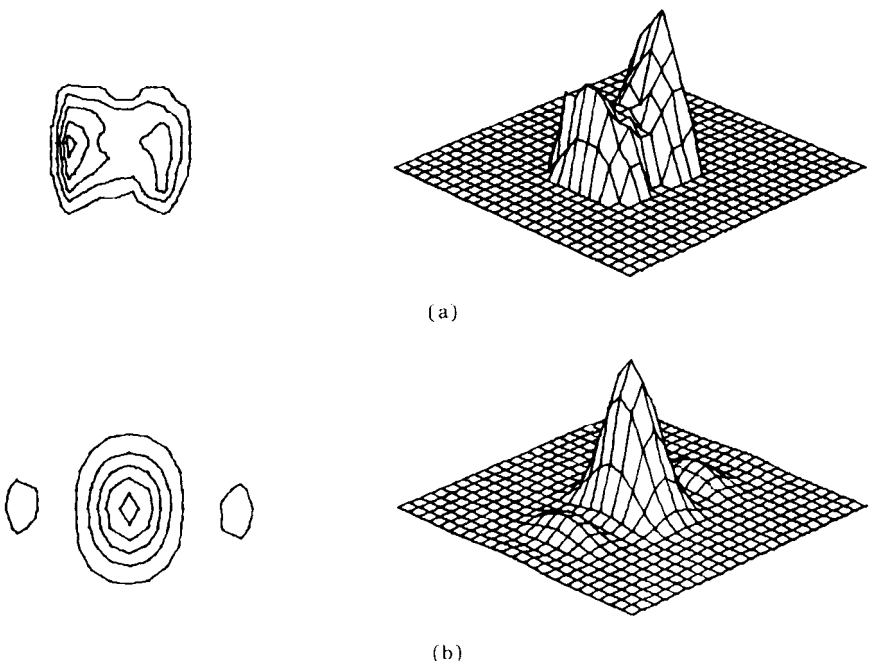

FIGURE 7 Focal spot of an actual x-ray tube; (a) impulse response; (b) squared MTF.

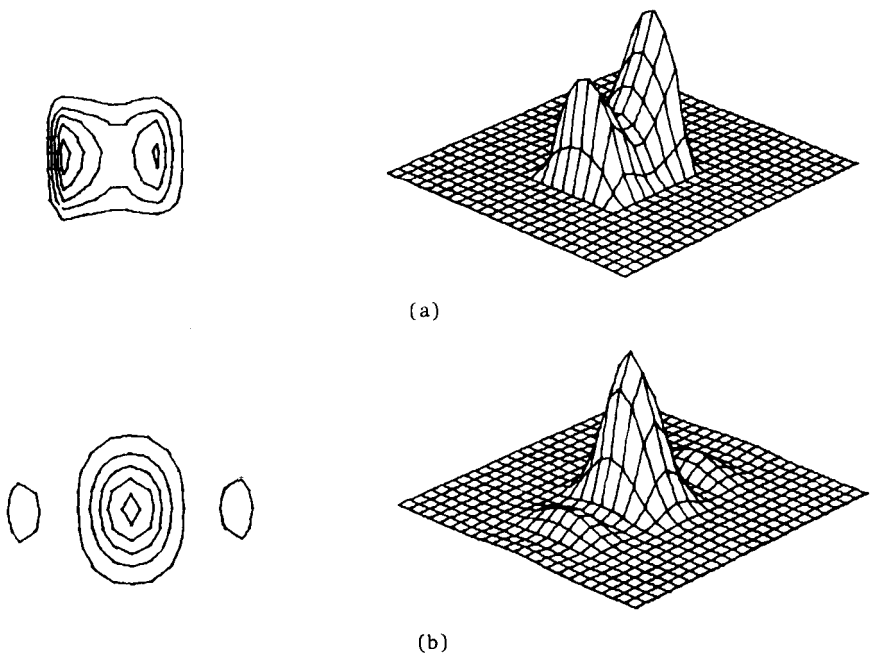

FIGURE 8 Approximation of the focal spot in Fig. 7 by a separable function: (a) impulse response; (b) squared MTF.

56]) techniques. This chapter deals with the digital implementation only. It should be noted that the PSF $h(x_f, y_f)$ has to be measured only once for a given focal spot, because the tomographic filter transfer function $H_t(f_x, f_y)$ can be determined for any layer using the appropriate scaling factors [see (4) and (10)].

4.2. Noise Handling Techniques

The filtering operation is indicated in (16). Unfortunately, $H(f_x, f_y)$ may have zeros and $G(f_x, f_y)$ is usually corrupted by noise. Thus the filtered image would include a large amount of noise at spatial frequencies in the neighborhood of a zero of $H(f_x, f_y)$. If the zeros are located at frequencies which are higher than those where the relevant physiological information is contained, a low-pass filter will be sufficient. Otherwise, noise handling techniques are necessary. Many such techniques have been described in the literature (e.g., [49,78]). No comparative assessment of all these techniques is available, only subjective estimates in specific cases [79]. Inverse filtering is not the best (especially in the presence of noise), but it is the simplest. Since our goal was not the determination of the best method

of image restoration, but to test the feasibility of tomographic filtering, we used a simple technique which provides a means for hard-limiting the magnitude response of the inverse filter while preserving the phase response and cutting off the high frequencies dominated by noise. The phase response should always be preserved because it is very important in images [72]. Both the hard limit and cutoff frequency can be specified by the user.

The goal is to design a filter whose transfer function $\bar{H}_t(f_x,f_f)$ is a modified version of $H_t(f_x,f_y)$ as shown in (10), in order to satisfy the constraints:

1. The magnitude response is limited:

$$|\bar{H}_t(f_x,f_y)| \leq H_L \tag{19}$$

2. The phase response is the same:

$$\sphericalangle \bar{H}_t(f_x,f_y) = \sphericalangle H_t(f_x,f_y) \tag{20}$$

This is accomplished by defining $\bar{H}_t(f_x,f_y)$ as follows [see (10)]:

$$\bar{H}_t(f_x,f_y) = \begin{cases} \dfrac{1}{H(f_x,f_y)} & \text{for } \dfrac{1}{|H(f_x,f_y)|} \leq H_L \quad (21) \\ H_L + j0 & \text{for } |H(f_x,f_y)| = 0 \quad (22) \\ H_L \dfrac{\mathrm{Re}[H(f_x,f_y] - j\mathrm{I}_m[H(f_x,f_y)]}{H(f_x,f_y)} & \text{for } \dfrac{1}{|H(f_x,f_y)|} > H_L \quad (23) \end{cases}$$

Equations (21) to (23) are consistent with (19) and (20); that is, the phase response is preserved and the dynamic range of the magnitude response can be controlled with the parameter H_L to prevent noise amplification and overflow of computer registers. In a digital computer all these operations are straightforward and they have been coded in FORTRAN routines [25]. Examples of applications are given below. It should be noted that under the transformations (20)-(22) a real PSF remains real, and an even PSF remains even.

Since the system transfer function usually has a low-pass characteristic, the inverse filter has a high-pass characteristic. Therefore, it is convenient to cascade the inverse filter with a low-pass filter to reduce the noise at high frequencies where the gain of the inverse filter is greatest. The choice of the cutoff frequency of the low-pass filter is a trade-off between the desired resolution and noise.

To design and implement the tomographic filter in (10), any other restoration filtering technique could have been used [49]. For example, Wiener filtering techniques have been applied to the design of digital tomographic filters [80].

4.3. Two-Dimensional Digital Filter Design

During this research the windowing technique for designing two-dimensional finite impulse response (FIR) filters was chosen because it can easily be used to approximate a completely arbitrary complex frequency response, such as that of a tomographic filter as given in (10). This includes both the magnitude and the phase responses. The argument justifying the use of the windowing technique is similar to that for the use of inverse filtering: during this research the parameters of the tomographic filters were changed frequently, thus a simple design technique was justified for this initial work. In future research, optimized two-dimensional IIR filters may prove more adequate.

The process of determining the digital filter coefficients can be described with reference to Fig. 9. This figure shows one-dimensional functions only, because the two-dimensional filters used were separable. Nevertheless, the same procedure would apply to nonseparable filters because the extension of the windowing technique to two dimensions is straightforward [25]. Figure 9a shows the magnitude response of the ideal inverse filter, as in (10). During this step, a correction by interpolation may be included if the sampling intervals of the PSF, $h(x_f,y_f)$, are not equal to those of the digitized radiograph. From the plot in Fig. 9a, a suitable hard limit is chosen and by applying the transformations (20) to (22) the filter in Fig. 9b is obtained. During this research the hard limits were selected by trial and error; however, they could eventually be predetermined for a given system in order to produce optimum results.

Figure 9c shows the effect of introducing a low-pass filter to reduce the noise at high frequencies, as discussed previously. Figure 9d shows the impulse response of this filter. The windowing technique can now be applied to determine the digital filter coefficients. The Kaiser window [82] was chosen not only because of its optimal behavior but also because it contains a parameter β that controls the frequency response trade-off between resolution and ripple.

A high β, such as $\beta = 9$, was used in order to obtain low ripples and a smooth transition band. Figure 9f shows the result of multiplying the impulse response in Fig. 9d by the Kaiser window in Fig. 9e. Finally, the FFT is used to obtain the coefficients of the tomographic filter in a form suitable for fast convolution realizations. The magnitude response of the tomographic filter is shown in Fig. 9g and h. An example of a tomographic filter that was actually used is shown in Fig. 10. This filter was obtained by multiplying two one-dimensional digital filters. Source listings of the computer programs (FORTRAN) used throughout this research can be found in [25].

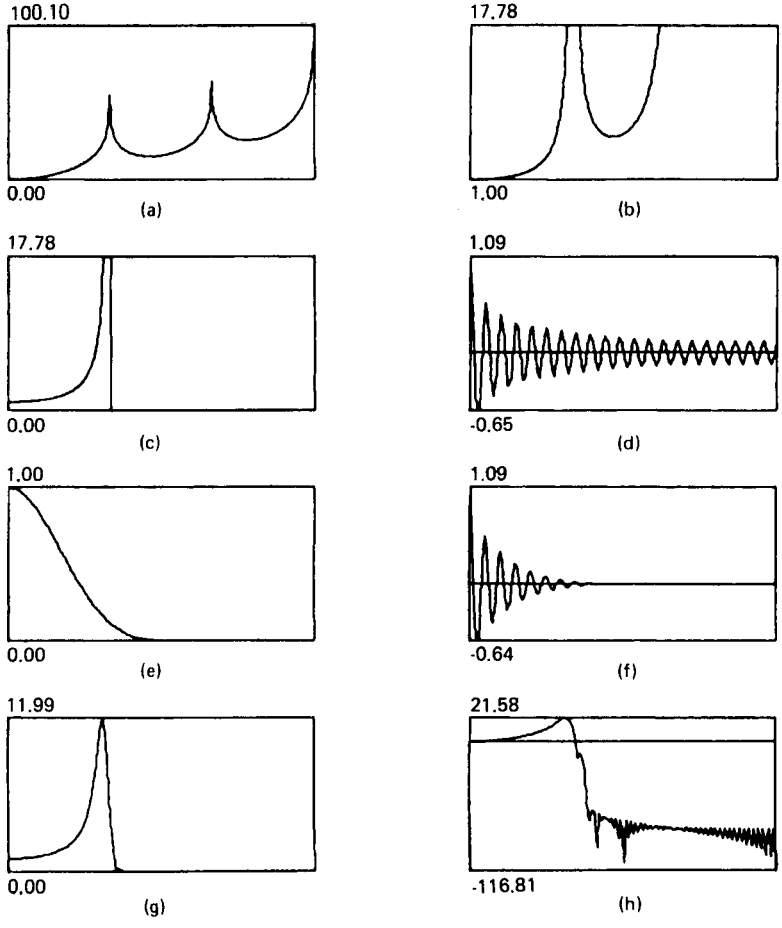

FIGURE 9 Plots of relevant functions at each step of the design of a a digital tomographic filter using the windowing technique (one dimension shown only): (a) magnitude response of the ideal inverse filter (in decibels); (b) inverse filter in part (a) with hard-limited magnitude response; (c) filter in part (b) cascaded with an ideal low-pass filter; (d) impulse response of the filter in part (c); (e) Kaiser window with $\beta = 9$; (f) windowed impulse response [part (d)] multiplied by part (e); (g) magnitude response of the tomographic filter; (h) the same magnitude response in decibels. (From Refs. 25 and 81.)

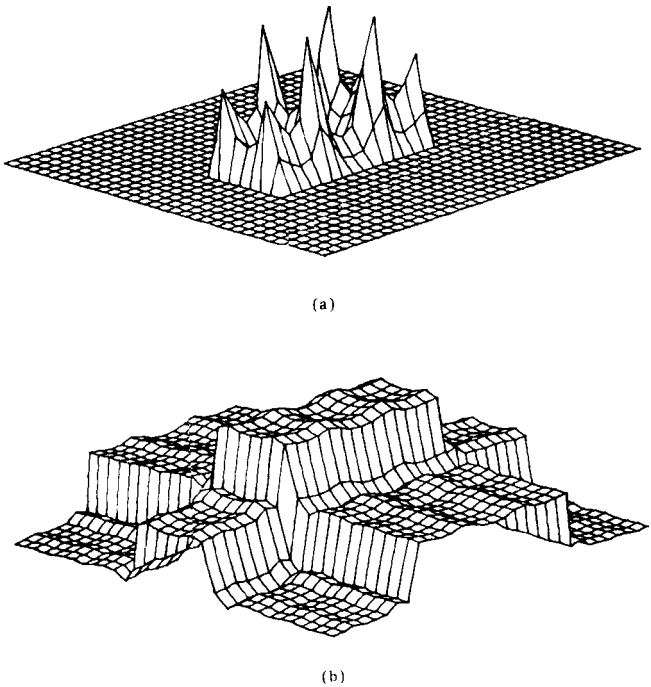

FIGURE 10 Typical tomographic filter; (a) magnitude response; (b) magnitude response in decibels.

4.4. Implementation and Examples

Filtering the data is the simplest operation in the whole process, although it is the one that requires the most CPU time. A portion of the radiograph to be processed is chosen and multiplied by a two-dimensional cosine taper data window to reduce the effects of leakage [25]. It is then Fourier-transformed using a two-dimensional FFT. The size 256 × 256 was found to give a good trade-off between resolution and cost for these experiments. The transform of the radiograph and the filter coefficients are complex-multiplied point by point. The result is inverse-transformed, quantized to 6 bits, and stored ready for display.

Three types of experiments were carried out to evaluate practically the performance of tomographic filters. For the first two, the radiologic system was simulated in a digital computer by approximating the image formation equations in the space domain [25]. This approach provided flexibility in the choice of focal spot shapes and object characteristics. Two

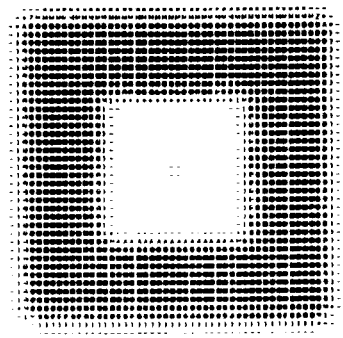

(a)

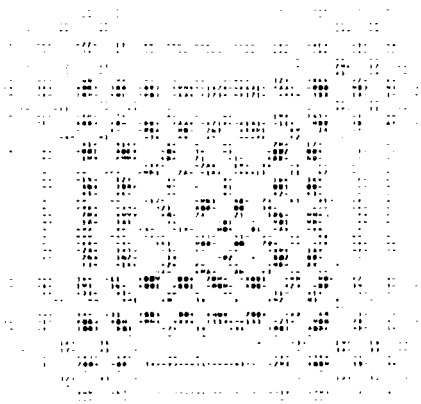

(b)

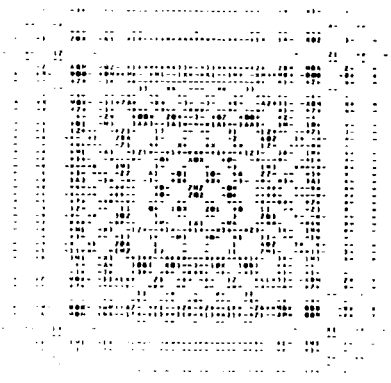

(c)

FIGURE 11 Experiments with thin objects: single-layer object with 100%/0% absorption located at 400 mm from the film plane. (a) Simulated radiograph of this object using a gaussian focal spot. (b)-(g) Results of processing part (a) with digital tomographic filters designed for the following depths (distances from the film plane): (b) 600 mm; (c) 550 mm; (d) 500 mm; (e) 450 mm; (f) 400 mm; (g) 350 mm.

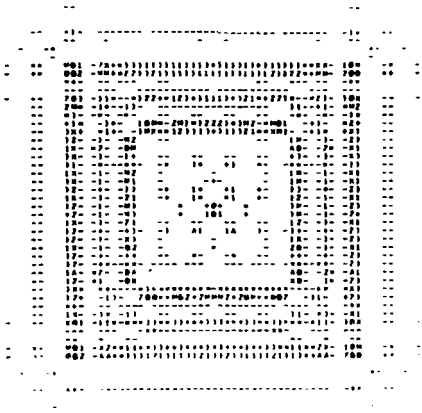

(d)

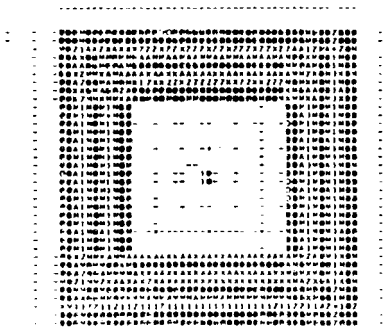

(e)

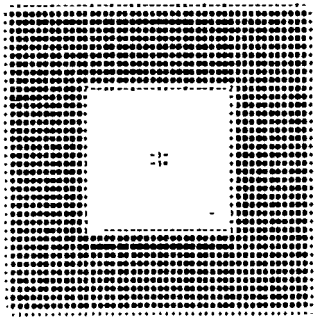

(f)

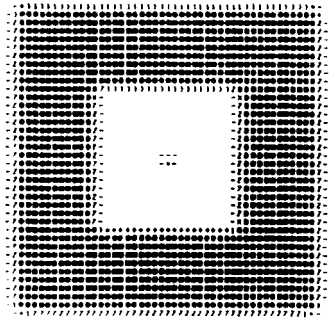

(g)

types of objects were simulated: "thin" objects (single layer) and a three-dimensional object composed of only two layers at different depths. Pictorial results of these simulations are reported below. The third type of experiment used actual radiographs. The radiographs were digitized and the impulse response of the system was calculated, as discussed previously [25].

Figure 11 shows the result of an experiment with a thin object (single layer) to see better the effect of tomographic filtering at various depths. This radiograph (Fig. 11a was simulated using a gaussian focal spot. The focal spot-to-film distance of the simulated system was 1000 mm. The object had 100% absorption, an aperture in the shape of a squarelike annulus, and a small hole in the center to obtain the impulse response. Each image has 128 × 128 pixels. Figure 11b-e clearly show the high-pass effect when a filter designed for one layer is used on another layer located closer to the film (see Fig. 5). The breakdown of unwanted structures is dramatic, although in practical applications the added source of noise may hinder the view of other layers.

Figure 11f shows the result when a single layer is in focus by the tomographic filter. The image in Fig. 11g contains blur because of the low-pass characteristics of the overall transfer function (see Fig. 5).

To observe the effect of layer superpositions, with the tomographic filter acting simultaneously on all layers, a three-dimensional object was composed by having parts of a star test pattern at two different levels and oriented at 90° with respect to one another. Figure 12a shows a simulated radiograph obtained with a gaussian focal spot. The focal spot-to-film distance was 1000 mm and the two layers of the object were positioned at depths (distance from the film) of 400 mm and 600 mm. The absorption in the object was 50%.

Figure 12b shows a simulation of an x-ray image obtained with a punctual focal spot. It has a blocklike structure, not visible in the other simulated radiograph because it is smeared by the blur. The object absorption in this case was 100%.

Figures 12c-d show the two-dimensional Fourier transforms of the images in Figs. 12a-b, respectively. Figure 13 shows the results of filtering Fig. 12a with digital tomographic filters. Magnitude-response hard limits and cutoff frequencies were applied to reduce the effects of noise. The values of the hard limits and cutoff frequencies were chosen by trial and error in these experiments. In Figs. 13a-b the objective is to recover the layer at 600 mm from the film (horizontal bars), but it was not possible to eliminate the image of the other layer. In Figs. 13c-d the objective is to recover the layer at 400 mm from the film (vertical bars) and the results are better. The effects of tomographic filtering are particularly good in Fig. 13d, where the blocklike structure of the vertical bars has been recovered well and the other layer (vertical bars) is not so clear. Thus we can conclude that tomographic filtering is easier when the layer of interest is closer to the film.

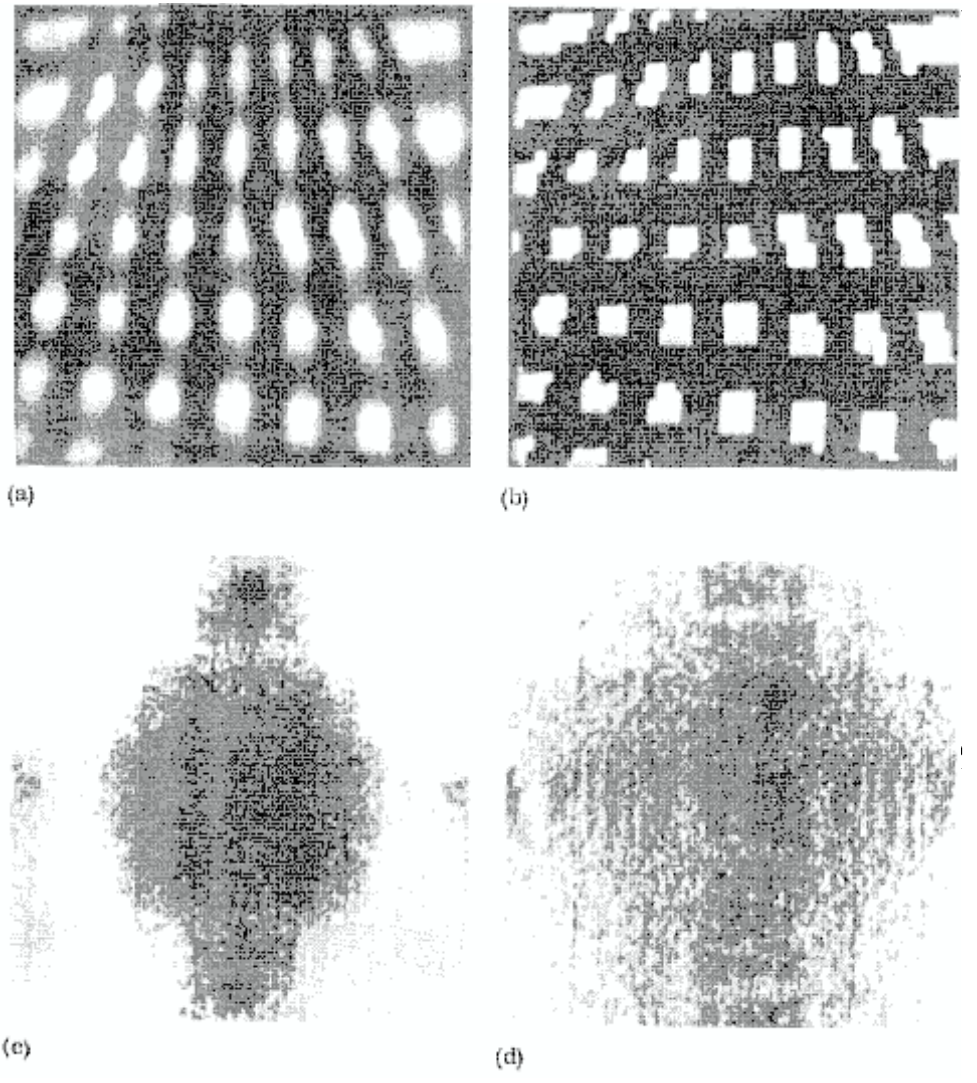

FIGURE 12 Experiments with thick objects: two-layer object with layers located at 600 mm and 400 mm from the film plane: (a) simulated radiograph of this object (50%/0% absorption) obtained with a gaussian focal spot; (b) simulated radiograph of this object (100%/0% absorption) obtained with a point source; (c)-(d) images representing the logarithm of the magnitude of the two-dimensional Fourier transform of the images in parts (a) and (b), respectively.

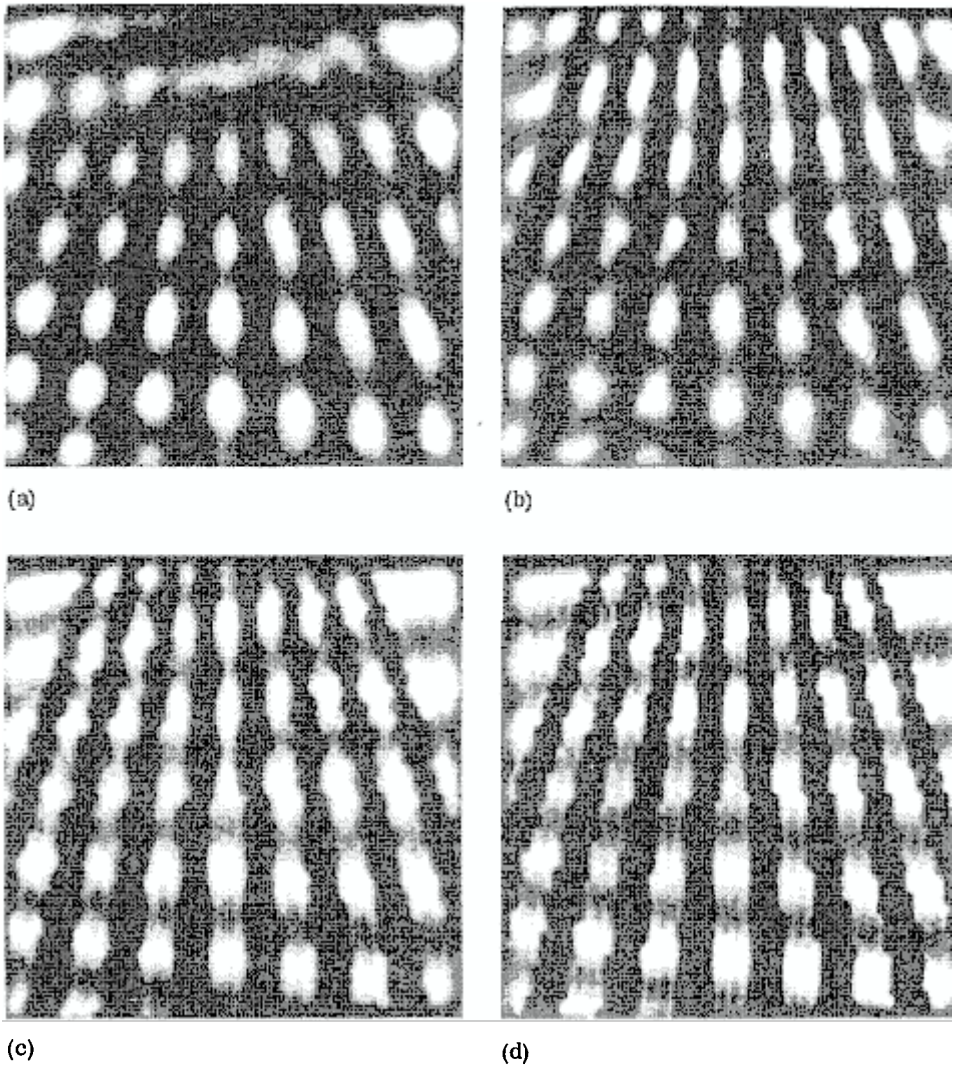

FIGURE 13 Results of filtering the radiograph in Fig. 12a with digital tomographic filters. Filters designed to recover the layer farthest away from the film: (a) filter with minimum gain of 10 dB; (b) filter with maximum gain of 20 dB. Filters designed to recover the layer closest to the film: (c) filter with maximum gain of 20 dB; (d) filter with maximum gain of 40 dB.

More examples of digital tomographic filters for radiographs can be found in [25,73,76,83,84]. In particular, the experiments with actual radiographs consisted of radiographs of a phantom chest with lesions on either side of the chest [25]. After processing these radiographs with tomographic filters, the image of a lesion tended to disappear when its depth did not coincide with the depth of the tomographic filter. This would permit determining the depth at which this lesion lies. Nevertheless, more research is necessary with actual radiographs to determine possible medical applications of tomographic filters.

5. CONCLUSIONS AND DIRECTIONS FOR FURTHER RESEARCH

In this chapter the problem of obtaining three-dimensional information by means of x rays has been discussed. The principal techniques used for that purpose have been reviewed briefly. A new technique, referred to as tomographic filtering or TFP, has been described. The idea is to filter conventional radiographs for the simulation of standard tomography, based on the finite size of the focal spot.

It has been shown that a TFP has a low-pass filter effect on the images of layers between the plane of cut and the focal spot and a high-pass effect on the images of layers between the plane of cut and the film. The performance of tomographic filters has been compared with standard tomography and conventional radiology. The theoretical and practical evaluations of the performance of tomographic filters have shown that the image-quality results cannot be as good as those of standard tomography in terms of the thickness of the tomographic layer, but they represent an improvement over conventional radiology. Tomographic filters allow the image analyst to interact with the system to exploit its capabilities, rather than being a passive observer of an image. The greatest advantage of a TFP is in reducing the radiation dose to the patient. Indeed, with a single radiograph and tomographic filtering operations of different parameters, additional depth information can be recovered without increasing the patient dose. Since tomographic filters can be implemented without the use of any special-purpose x-ray hardware, they extend the utility of conventional radiology equipment.

More research is required to determine possible clinical applications of tomographic filtering, as well as to optimize their design and implementation. A few possible directions follow.

Since the performance of tomographic filtering depends on the characteristics of the human body, such as position and size of lesions, overlaying and underlaying structures (e.g., ribs), exposure, geometry, direction of the projection, and so on, the medical evaluation of tomographic filtering should take these variables into account in order to determine for what applications (e.g., type of disease, organ, lesions) tomographic filtering could

complement other methods in the medical imaging hierarchy. Medical image information quality standards are needed so that rules can be set for calibration of experiments and the results of experiments can be judged accordingly. The peculiarities of the tomographic filtering process, such as the high-pass effect between the plane of cut and the film, need to be investigated further with respect to the diagnostic quality of the processed radiograph. The influence of the type of focal spot [i.e., the exposure function $I_0(x_0,y_0)$] could also be investigated taking into account the trade-offs: for example, larger focal spots give better depth resolution but restoration is more difficult.

Another area is the design of digital tomographic filters. Filter structures, such as homomorphic, Wiener, and various modifications of inverse filtering, could be evaluated to determine their suitability for tomographic filtering. The use of recursive techniques for digital tomographic filters could be investigated, because "recursive tomographic filters" would probably use less computer memory and time in their implementation. Filter parameters such as the order of the tomographic filter, computer word length, mode of arithmetic, and round-off errors would influence both the cost and the quality of the results; thus trade-offs should be determined.

Finally, extensions of this research can be suggested. It might be possible to identify the blur characteristics from the radiograph itself, using the techniques of power spectrum and power cepstrum estimation. The use of tomographic filtering might be useful as a preprocessing technique for automated pattern recognition processes. Tomographic filtering may also have applications in standard tomography, in order to change the plane of cut of a tomogram by means of tomographic filtering. The tomographic filtering concept might be useful in other areas, such as geophysics, nuclear imaging, astronomy, ultrasound, and photography.

REFERENCES

1. B. G. Ziedses des Plantes, Body-section radiography: History, image information, various techniques and results, Australasian Radiol., vol. 15, pp. 57-64, Feb. 1971.
2. W. J. Meredith and J. B. Massey, Fundamental Physics of Radiology, 2nd ed., John Wright & Sons, Bristol, England, 1972.
3. A. Berrett, S. Brünner, and G. E. Valvassory (Eds.), Modern Thin-Section Tomography, Charles C Thomas, Springfield, Ill., 1973.
4. H. H. Barrett and W. Swindell, Radiological Imaging, Academic Press, New York, 1981.
5. E. R. Miller, E. M. McCurry, and B. Hruska, An infinite number of laminagrams from a finite number of radiographs, Radiology, vol. 9, pp. 249-255, Feb. 1971.

6. D. G. Grant, Tomosynthesis: A three dimensional radiographic imaging technique, IEEE Trans. Biomed. Eng., vol. BME-19, pp. 20-28, 1972.
7. M. Kock and U. Tiemens, Tomosynthesis: A holographic method for variable depth display, Opt. Commun., vol. 7, pp. 260-265, 1973.
8. P. Edholm and L. Quiding, Elimination of blur in linear tomography, Acta Radiol. (Diag.), vol. 10, pp. 441-447, 1970.
9. J. W. Strohbehn, C. H. Yates, B. H. Curran, and E. S. Sternick, Image enhancement of conventional transverse-axial tomograms, IEEE Trans. Biomed. Eng., vol. BME-26, pp. 253-262, May 1979.
10. M. W. Vannier and R. G. Jost, Digital processing of conventional tomograms, Appl. Opt. Instrum. Med. IX, Proc. SPIE, vol. 273, pp. 350-356, 1981.
11. P. Levy, The analysis and processing of medical tomograms, Ph.D. thesis, University of Reading, Reading, England, 1977.
12. R. A. Robb, X-ray computed tomography: An engineering synthesis of multiscientific principles, CRC Crit. Rev. Biomed. Eng., vol. 7, pp. 265-333, 1982.
13. R. M. Mersereau, Digital reconstruction of two-dimensional signals from their projections, Sc.D. dissertation, Dept. of Electrical Engineering. Massachusetts Institute of Technology, Cambridge, Mass., Feb. 1973.
14. R. M. Mersereau and A. V. Oppenheim, Digital reconstruction of multidimensional signals from their projections, Proc. IEEE, vol. 62, pp. 1319-1338, 1974.
15. Special Issue on Technology and Health Care, Proc. IEEE, vol. 67, pp. 1185-1361, Sept. 1979.
16. Special Issue on Computerized Tomography, Proc. IEEE, vol. 71, pp. 289-435, Mar. 1983.
17. M. R. Rangaraj and R. Gordon, Computed tomography for remote areas via teleradiology, First Int. Conf. Workshop Picture Archiving Commun. Syst. (PACS) Med. Appl., Proc. SPIE, vol. 318, pp. 182-185, 1982.
18. H. H. Barrett, K. Garewal, and D. T. Wilson, A spatially-coded x-ray source, Radiology, vol. 104, pp. 429-430, Aug. 1972.
19. H. H. Barrett and W. Swindell, Analog reconstruction methods for transaxial tomography, Proc. IEEE, vol. 65, pp. 89-107, Jan. 1977.
20. H. J. Trussell, Processing of x-ray images, Proc. IEEE, vol. 69, pp. 615-627, May 1981.
21. Digital Radiogr., Proc. SPIE, vol. 314, 1981.
22. First Int. Conf. Workshop Picture Archiv. Commun. Syst. (PACS) Med. Appl., Proc. SPIE, vol. 318, 1982.
23. S. J. Dwyer III (Ed.), 2nd Int. Conf. Workshop Picture Archiv. Commun. Syst. (PACS II) Med. Appl., Proc. SPIE, vol. 418, 1983.

24. Special Issue on Digital Image Archiving in Medicine, Computer, vol. 16, pp. 14-56, Aug. 1983.
25. J. M. Costa, Design and realization of digital tomographic filters for radiographs, Ph.D. dissertation, University of Toronto, Toronto, Ontario, 1981.
26. K. Rossman, Image quality, Radiol. Clin. North Am. (Symp. Perception of the Roentgen Image), vol. 7, pp. 419-433, Dec. 1969.
27. E. M. Laasonen, Information transmission in Roentgen diagnostic chains, Acta Radiol., Suppl. 280, pp. 1-93, 1968.
28. R. H. Morgan, The frequency response function, a valuable means of expressing the informational recording capability of diagnostic x-ray systems, Am. J. Roentgenol., Radiat. Ther. Nuclear Med., vol. 88, pp. 175-186, July 1962.
29. K. Doi, A. Kaji, T. Takizawa, and K. Sayanagi, The application of optical transfer function in radiography, Proc. Conf. Photogr. Spectrosc. Opt., 1964, Jap. J. Appl. Phys., vol. 4, Suppl. I, pp. 183-190, 1965.
30. R. D. Moseley, Jr., and J. H. Rust (Eds.), Diagnostic Radiologic Instrumentation, Modulation Transfer Function, Charles C Thomas, Springfield, Ill., 1965.
31. G. T. Barnes, Radiographic mottle: A comprehensive theory, Med. Phys., vol. 9, pp. 656-667, Sept./Oct. 1982.
32. J. M. Costa, A. N. Venetsanopoulos, and M. Trefler, Digital tomographic filtering of radiographs, IEEE Trans. Med. Imaging, vol. MI-2, pp. 76-88, June 1983.
33. N. C. Beese, The focusing of electrons in an x-ray tube, Rev. Sci. Instrum., vol. 8, N.S., pp. 258-262, July 1937.
34. E. Takenaka, K. Kinoshita, and R. Nakajima, Modulation transfer function of the intensity distribution of the Roentgen focal spot, Acta Radiol. Ther. Phys. Biol., vol. 7, Fasc. 4, pp. 263-272, Aug. 1968.
35. K. Doi, Optical transfer functions of the focal spot of x-ray tubes, Am. J. Roentgenol. Radiat. Ther. Nuclear Med., vol. 94, pp. 712-718, July 1965.
36. G. Lubberts and K. Rossmann, Modulation transfer function associated with geometrical unsharpness in medical radiography, Phys. Med. Biol., vol. 12, pp. 65-67, Jan. 1967.
37. R. F. Wagner, K. E. Weaver, E. W. Denny, and R. G. Bostrom, Toward a unified view of radiological imaging systems: Part I. Noiseless images, Med. Phys., vol. 1, pp. 11-24, Jan-Feb. 1974.
38. E. L. Chaney and W. R. Hendee, Effects of x-ray tube current and voltage on effective focal-spot size, Med. Phys., vol. 1, pp. 141-147, May-June 1974.
39. G. U. V. Rao and A. Soong, An intercomparison of the modulation transfer functions of square and circular focal spots, Med. Phys., vol. 1, pp. 204-209, July-Aug. 1974.

40. K. Doi and K. Sayanagi, Role of optical transfer function for optimum magnification in enlargement radiography, Jap. J. Appl. Phys., vol. 9, pp. 834-839, July 1970.
41. J. E. Gray and M. Trefler, Phase effects in diagnostic radiological images, Med. Phys., vol. 3, pp. 195-203, July-Aug. 1976.
42. S. Wende, E. Zieler, and N. Nakayama, Cerebral Magnification Angiography, Springer-Verlag, New York, 1974, Chap. 8.
43. M. P. Capp, Radiological imaging—2000 A.D., Radiology, vol. 138, pp. 541-550, Mar. 1981.
44. B. R. Hunt, Digital image processing, Proc. IEEE, vol. 63, pp. 693-708, Apr. 1975.
45. D. G. Falconer, Image enhancement and film-grain noise, Opt. Acta, vol. 17, pp. 693-705, Sept. 1970.
46. B. R. Hunt and J. R. Breedlove, Scan and display considerations in processing images by digital computer, IEEE Trans. Comput., vol. C-24, pp. 848-853, Aug. 1975.
47. L. Biberman (Ed.), Perception of Displayed Information, Plenum Press, New York, 1973.
48. A. Rose, A unified approach to the performance of photographic film, television pickup tubes, and the human eye, J. Soc. Motion Picture Eng., vol. 47, pp. 273-294, Oct. 1946.
49. H. C. Andrews and B. R. Hunt, Digital Image Restoration, Prentice-Hall, Englewood Cliffs, N.J., 1977.
50. H. C. Andrews, Monocrome digital image enhancement, Appl. Opt., vol. 15, pp. 495-503, Feb. 1976.
51. R. H. Selzer, Improving biomedical image quality with computers, Tech. Rep. 32-1336, Jet Propulsion Laboratory, Pasadena, Calif., Oct. 1, 1968.
52. P. W. Hesse, Fourier transform enhancement of radiographs, Proc. 8th Symp. Nondestructive Eval. Aerosp. Weapons Syst. Nuclear Appl., Apr. 21-23, 1971, pp. 155-167.
53. B. R. Hunt, D. H. Janney, and R. K. Zeigler, An introduction to restoration and enhancement of radiographic images, Tech. Rep. LA-4305, Los Alamos Scientific Laboratory, Los Alamos, N.M., 1970.
54. B. R. Hunt, The inverse problem of radiography, Math. Biosci., vol. 8, pp. 161-179, 1970.
55. J. B. Minkoff, S. K. Hilal, W. F. Konig, M. Arm, and L. B. Lampert, Optical filtering to compensate for degradation of radiographic images produced by extended sources, Appl. Opt., vol. 7, pp. 663-641, 1968.
56. G. A. Krusos, The amelioration of contrast and resolution of x-ray images using optical signal processing, Eng. Sc.D. dissertation, Columbia University, New York, 1971.

57. M. Trefler and E. N. C. Milne, The diagnostic quality of optically processed radiographs, Radiology, vol. 121, pp. 211-213, Oct. 1976.
58. E. L. Hall, Digital filtering of images, Ph.D. dissertation, University of Missouri, Columbia, Jan. 1971.
59. E. L. Hall, R. P. Kruger, S. J. Dwyer, III, D. L. Hall, R. W. McLaren, and G. S. Lodwick, A survey of preprocessing and feature extraction techniques for radiographic images, IEEE Trans. Comput., vol. C-20, pp. 1032-1044, Sept. 1971.
60. S. C. Orphanoudakis and J. W. Strohbehn, Mathematical model of conventional tomography, Med. Phys., vol. 3, pp. 224-232, July-August 1976.
61. S. C. Orphanoudakis, J. W. Strohbehn, and C. E. Metz, Linearizing mechanisms in conventional tomographic imaging, Med. Phys., vol. 5, pp. 1-7, Jan.-Feb. 1978.
62. J. M. Costa, Insight into radiological imaging, Proc. First IASTED Symp. Appl. Inf., Lille, France, vol. I, pp. 189-192, March 15-17, 1983.
63. H. J. Trussell and B. R. Hunt, Image restoration of space-variant blurs by sectioned methods, IEEE Trans. Acoust. Speech Signal Process., vol. ASSP-26, pp. 608-609, Dec. 1978.
64. M. Trefler and J. E. Gray, Characterization of the imaging properties of x-ray focal spots, Appl. Opt., vol. 15, pp. 3099-3104, Dec. 1976.
65. L. C. Baird, How big is a pinhole? Med. Phys., vol. 7, p. 64, Jan./Feb. 1980.
66. E. N. C. Milne, The role and performance of minute focal spots in roentgenology with special reference to magnification, CRC Crit. Rev. Radiol. Sci., vol. 2, pp. 269-310, May 1971.
67. D. Westra, Zonography—The narrow-Angle Tomography, Excerpta Medica Foundation, Amsterdam, 1966.
68. K. Lindblom, On microtomography, Acta Radiol. (Stockholm), vol. 42, p. 465, 1954.
69. P. Edholm, The tomogram, its formation and content, Acta Radiol. (Stockholm), Supplementum 193, 1960.
70. T. G. Stockham, Jr., Image processing in the context of a visual model, Proc. IEEE (Special Issue on Digital Picture Processing), vol. 60, no. 7, pp. 828-842, July 1972.
71. B. S. Lipkin and A. Rosenfeld (Eds.), Picture Processing and Psychopictorics, Academic Press, New York, 1970.
72. T. S. Huang, J. W. Burnett, and A. G. Deczky, The importance of phase in image processing filters, IEEE Trans. Acoust. Speech Signal Process., vol. ASSP-23, pp. 529-542, Dec. 1975.
73. J. M. Costa, Medical image communication systems, Digital Radiogr., Proc. SPIE, vol. 314, pp. 380-388, 1981.
74. J. M. Costa, Tomographic filters for digital radiography, Digital Radiogr., Proc. SPIE, vol. 314, pp. 64-71, 1981.

75. J. M. Costa, A. N. Venetsanopoulos, and M. Trefler, Evaluation of digital tomographic filters, IEEE Trans. Med. Imaging, vol. MI-4, pp. 1-13, March 1985.
76. J. M. Costa, A. N. Venetsanopoulos, and M. Trefler, Design and implementation of digital tomographic filters, IEEE Trans. Med. Imaging, vol. MI-2, pp. 89-100, June 1983.
77. M. Maue-Dickson and M. Trefler, Image quality in computerized and conventional tomography in the assessment of craniofacial anomalies, University of Miami School of Medicine, Miami, Fla., Aug. 26, 1977.
78. M. M. Sondhi, Image restoration: The removal of spatially invariant degradations, Proc. IEEE, vol. 60, pp. 842-853, July 1972.
79. B. R. Hunt and H. C. Andrews, Comparison of different filter structures for image restoration, Proc. 6th Annu. Hawaii Int. Conf. Syst. Sci., Jan. 1973.
80. G. Mitsiadis and A. N. Venetsanopoulos, Design of digital tomographic filters, Proc. Mediterranean Electrotech. Conf. (Melecon '83), Athens, 24-26 May 1983, paper C2.02.
81. J. M. Costa and A. N. Venetsanopolous, Digital tomographic restoration of radiographs, Proc. Conf. Digital Process. Signals Commun., University of Technology, Loughborough, Leicestershire, England, IERE Conf. Proc. 37, pp. 559-567, Sept. 6-8, 1977.
82. J. F. Kaiser, Nonrecursive digital filter design using the I_0-sinh window function, Proc. 1974 IEEE Symp. Circuits Syst., pp. 20-23, Apr. 22-25, 1974.
83. J. M. Costa and A. N. Venetsanopoulos, Digital filtering for the extraction of three-dimensional information from a single radiograph, Proc. Int. Conf. Digital Signal Process., Florence, pp. 930-937, Sept. 2-5, 1981.
84. J. M. Costa and A. N. Venetsanopoulos, Tomographic filters, Proc. Int. Electr. Electron. Conf. Expos., Toronto, Ontario, Sept. 26-28, 1983, pp. 530-533.